

Properties of Iron and Steel Slag Hydrated Matrix Exposed in Sea Area for Long Period[†]

INOUE Yotaro*¹ MATSUNAGA Hisahiro*² WATANABE Keiji*³

Abstract:

“FerroformTM”, iron and steel slag hydrated matrix, consisting mainly of steelmaking slag as aggregate and ground granulated blast furnace slag as binder, were exposed in sea area for 10 years and were examined. Many organisms were confirmed on the surface of samples at undersea zone. The compressive strength of test sample was 27-30 N/mm², which is more than twice as high as same sample after standard curing for 4 weeks. The apparent Cl diffusion coefficient was 0.04-0.16 cm²/year at tidal zone and 0.3-0.5 cm²/year at undersea zone. The average neutralization depths at tidal zone was 2.5 mm, and the neutralization rate coefficient was smaller than that of ordinary portland cement concrete and slag cement concrete. Pore size was small, which is consistent with the results of small neutralization rate coefficient. Generation and eluviation of Friedel's salt, and condensation of SO₃ were confirmed.

1. Introduction

Iron and steel slag hydrated matrix, FerroformTM, is a slag product in which steelmaking slag is used as the aggregate and mainly ground granulated blast furnace slag is used as a binder, and makes it possible to produce structures by the same production flow as that used in general concrete products^{1,2)}. As a result, generation of CO₂ in the cement production process and environmental loads associated with gathering of natural aggregate can be suppressed. Iron and steel slag hydrated matrix can also be used as an artificial stone material called Frontier RockTM (hereinafter, “artificial stone”) when mixed at a specified mix proportion,

hardened and rough-crushed to pieces weighing up to 1 ton each with arbitrary diameters of 100 mm to more than 700 mm³⁾.

This report describes the results of a study of the changes in the properties of iron and steel slag hydrated matrix when exposed in an actual environment for a long period as artificial stones for seawall foot protection. The object of the study was artificial stones produced in September 2000 and installed in a seawater canal at West Japan Works (Kurashiki) of JFE Steel Corporation in January of 2001. The artificial stones were recovered in July 2010, approximately 9.5 years after exposure began. Various types of investigations were performed, and the properties of the artificial stones were compared with those of the conventional concrete, in which ordinary Portland cement or Portland blast-furnace slag cement was used.

2. Outline of Experiment

2.1 Materials Used and Mix Proportion

The specific mix proportion of artificial stone is shown in **Table 1**. The maximum dimension of the steelmaking slag used as the aggregate was 40 mm. Ground granulated blast furnace slag was used as the main binder material, lime dust was used as an alkali stimulus material, and fly ash was used as an admixture. The amount of CaO contributing to bonding in the lime dust was 50 wt%, and the water/binder ratio W/B was calculated considering that fact.

[†] Originally published in *JFE GIHO* No. 40 (Aug. 2017), p. 19-24



*¹ Senior Researcher Deputy Manager,
Slag & Refractories Research Dept.,
Steel Res. Lab.,
JFE Steel



*² Dr. Env.,
Senior Researcher Deputy General Manager,
Slag & Refractories Research Dept.,
Steel Res. Lab.,
JFE Steel



*³ Dr. Eng.,
General Manager,
Slag & Refractories Research Dept.,
Steel Res. Lab.,
JFE Steel

Table 1 Specific mix proportion

Max size of aggregate (mm)	Water-binder ratio (%)	Quantity of material per unit volume of concrete (kg/m ³)					
		Water	Aggregate: steel-making slag	Ground granulated blast-furnace slag	Fly-ash	Alkaline stimulus: lime dust	Admixture
40	43	265	1 360	340	244	70	2



Photo 1 Seawater canal in Kurashiki area

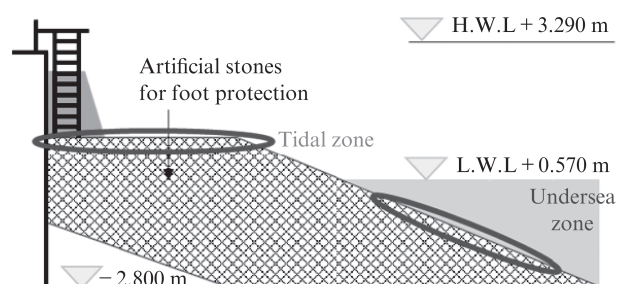


Fig. 1 Exposure conditions: tidal zone and undersea zone

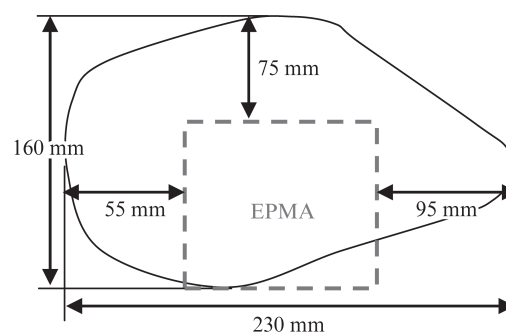
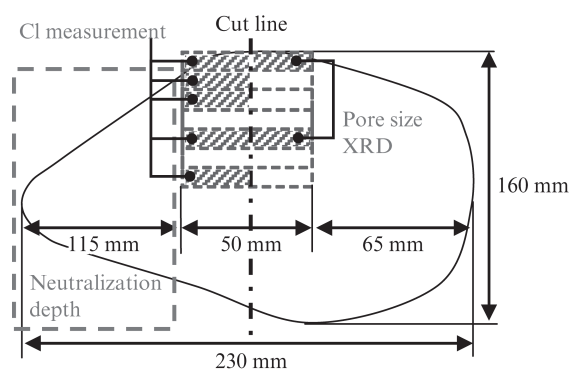


Fig. 2 Measurement points and measurement items of a sample at tidal zone

2.2 Sample Exposure Conditions and Recovery Conditions

The dimensions of the samples were 150–250 mm in diameter and 100–200 mm in height, and the shape of each stone was different. As shown in **Photo 1**, the artificial stones were used as foot protection stones of a seawater canal in JFE Steel West Japan Works (Kurashiki) in Kurashiki City, Okayama Prefecture. The average annual temperature is 16.0°C, and annual precipitation is 800 mm, which is smaller than the national average. As shown in the cross-sectional diagram in **Fig. 1**, the exposure environment was divided into two zones, an underwater zone and a tidal zone. About 10 stones were recovered from each zone 9.5 years after the start of exposure (material age: 9.75 years).

2.3 Measurement Items and Methods

Cores were taken from four stones each from the undersea zone and the tidal zone, and uniaxial compressive strength was measured. One stone from each zone was cut into two parts, and various properties

were evaluated. **Figure 2** shows the evaluation positions and evaluation items, using a sample exposed in the tidal zone as an example. The details of the property evaluations are described below.

- Chloride ion concentration: A specimen for analysis having dimensions of 25×10×20 mm was cut out in the depth direction, dried at 105°C and pulverized. Separately from this, the average chloride ion concentration of a 10 mm width in the vertical direction (depth direction), excluding the aggregate, was calculated from the elemental distribution results of the cross-sectional region at a comparatively flat part of the surface.
- Neutralization test: A phenolphthalein solution was sprayed on the left side of the central cross section of the tidal zone sample, and the neutralization depth was measured.
- Pore size distribution and powder X-ray diffraction: A 25×10×20 mm sample was cut out in the depth direction and then cut into two parts, and the pore size distribution and X-ray diffraction analysis were performed. The mercury intrusion porosimetry



Photo 2 Surface appearance of a sample at undersea zone

(MIP) method was used to obtain the pore size distribution. For powder X-ray diffraction, specimens were prepared after removing the aggregate as completely as possible.

- Element distribution (Cl, S, Si, Ca): An 80×80×20 mm specimen was cut out from the cross section of a comparatively flat part of the surface and used as a specimen for EPMA.

3. Experimental Results and Discussion

3.1 Appearance

Photo 2 shows the surface appearance of a sample exposed in the undersea zone immediately after recovery. A large number of adhering organisms were found, including lugworms, starfish, clams, barnacles, etc. From this, the artificial stone is considered to have excellent bioaffinity.

3.2 Compressive Strength

The results of measurements of uniaxial compressive strength are shown in Fig. 3. Since samples were taken from the tidal zone at a material age of 5 years and from the undersea and tidal zones at a material age of 7 years, those results are also shown in the same figure. Compressive strength shows an increasing ten-

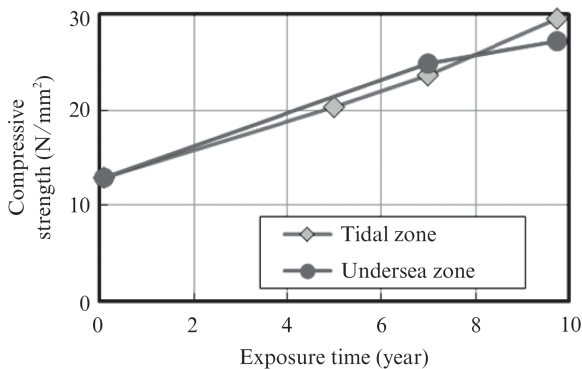


Fig. 3 Compressive strength of samples at tidal zone and undersea zone

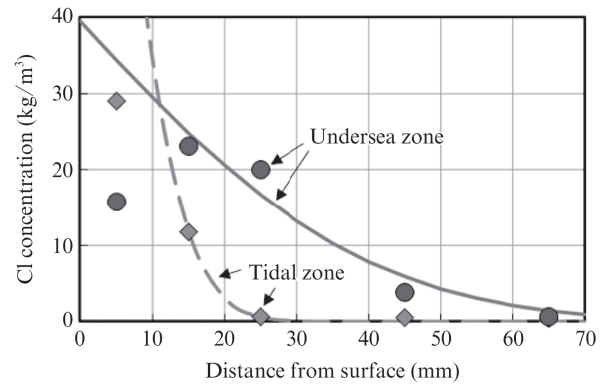


Fig. 4 Cl concentration distribution of samples at tidal zone and undersea zone

dency. According to a report⁴⁾ of an investigation of various types of concrete exposed to a marine environment for 10 years, the concretes that showed increases in compressive strength from before exposure to 10 years were one of two samples in which ordinary Portland concrete was used and three of three samples in which Portland blast-furnace slag cement was used. In contrast, increases in strength in comparison with standard curing (28 days) samples were observed with all levels of the artificial stones after exposure for 10 years. The results of an investigation of concrete exposed to a marine environment for 15 years showed that the strength increase rate after 15 years against 28-day strength became higher as the use ratio of ground granulated blast furnace slag increased⁵⁾. With iron and steel slag hydrated matrix, as with concrete, it is considered that the use ratio of ground granulated blast furnace slag influences these differences in the latent hydraulic property and seawater resistance.

3.3 Chloride Penetration

Chloride penetration was investigated in order to verify the applicability of iron and steel slag hydrated matrix as a substitute for steel reinforced concrete. The measurement results are shown in Fig. 4. The total chloride ion concentration at which corrosion of reinforcing steel in concrete occurs (chloride threshold value for initiation of corrosion in steel materials) differs depending on the type of cement and the water/cement ratio⁶⁾. Using the equation for type B ground granulated blast furnace slag and type B equivalent fly ash cement, the chloride threshold value with this mix proportion can be calculated as 1.98 kg/m³. In the tidal zone, the Cl concentration exceeded 1.98 kg/m³ to a depth of 20 mm from the material surface. On the other hand, from the measured values in the undersea zone, the Cl concentration exceeded 1.98 kg/m³ to a depth of 50 mm, showing that Cl penetration was deeper in the undersea zone than in the tidal zone. Because the seawater canal where the artificial stones

were exposed was located at a distance from the sea-coast, it was affected by tides but not by waves. Similar results have also been reported⁵⁾ in exposure in a circulation tank which approximated this condition; namely, Cl penetration was deeper in the simulated undersea zone than in the tidal zone.

Next, based on Eq. (1), the apparent Cl diffusion coefficient D including eluviation of salts, etc. from the surface was calculated. The calculated values of the Cl concentration obtained by fitting are also shown in Fig. 4. The Cl diffusion coefficient was 0.04 (cm²/yr) in the tidal zone and 0.48 (cm²/yr) in the undersea zone.

$$C(x,t) = C_0 \left\{ 1 - \operatorname{erf} \left(\frac{x}{2\sqrt{Dt}} \right) \right\} \dots\dots\dots (1)$$

- $C(x, t)$: chloride ion concentration (kg/m³)
- C_0 : chloride ion concentration at outermost surface (kg/m³)
- D : apparent Cl diffusion coefficient (cm²/yr)
- x : depth (cm)
- t : exposure time (years)
- erf : error function

The Cl concentration was also calculated from the EPMA results for different surface regions. In these calculations, the matrix excluding aggregate and pores was used. As in the chemical analysis, the results showed deeper Cl penetration in the undersea zone in comparison with the tidal zone. The diffusion coefficients were 0.16 (cm²/yr) in the tidal zone and 0.27 (cm²/yr) in the undersea zone.

The obtained Cl diffusion coefficients, D , were compared considering the water/binder W/B ratio. The results are shown in Fig. 5. N indicates concrete using ordinary Portland cement (hereinafter, N), and BB indicates concrete using ground granulated blast furnace slag (hereinafter, BB). The figure shows the results by the equation⁶⁾ of the Japan Society of Civil Engi-

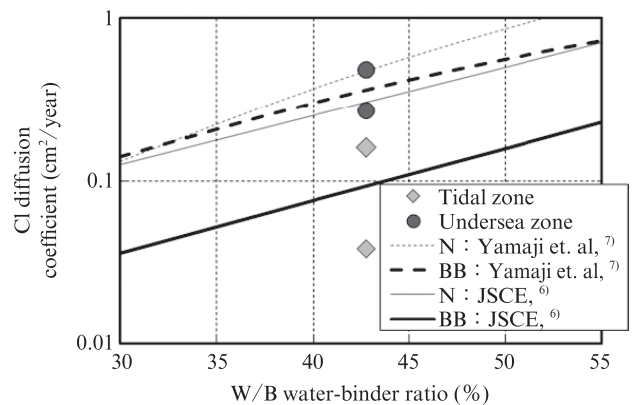


Fig. 5 Cl diffusion coefficient of samples at tidal zone and undersea zone

Table 2 Neutralization depth of a sample at tidal zone

Number of measurements	Neutralization depth (mm)			Neutralization rate coefficient (mm/√year)
	Min	Max	Ave	
42	0.0	5.5	2.5	0.81

neers (JSCE) and the equation proposed by Yamaji⁷⁾. In the tidal zone, the diffusion coefficients are equal to or lower than that of concrete using BB, and in the undersea zone, the results fall between those for concrete using N and concrete using BB. The fact that the diffusion coefficient in the undersea zone is somewhat large in comparison with the concrete using BB is considered to be due to the effect of the larger unit water content in comparison with the ordinary (N) concrete. Since the XRD results, which will be described in the following, also revealed the presence of unreacted fly ash, the influence of underestimation of W/B of the samples is conceivable.

3.4 Neutralization

The neutralization depth in the tidal zone was investigated. Table 2 shows the details of the measured results. The average neutralization depth was 2.5 mm. Next, the neutralization rate coefficient was calculated based on Eq. (2). The neutralization rate coefficient in the tidal zone was calculated as 0.81 mm/√yr.

$$L = a \sqrt{t} \dots\dots\dots (2)$$

- L : neutralization depth (mm)
- a : neutralization rate coefficient (mm/√yr)
- t : elapsed time (years)

In order to compare the neutralization rate coefficient with that of ordinary concrete, the effective water binder ratio W/B^* ⁸⁾ shown by Eq. (3) was calculated. Here, from the viewpoint of the alkaline fraction, the coefficient of slaked lime was assumed hypothetically to be equal to or larger than that of Portland cement, and was set at 1. Based on this assumption, the coefficient of lime dust was assumed to be 0.5 from the slaked lime content ratio (wt%).

$$W/B^* = W / (C_p + k \cdot A_d) \dots\dots\dots (3)$$

- W : mass of water per unit volume
- B^* : effective mass of binder per unit volume
- C_p : mass of Portland cement per unit volume
- A_d : mass of admixture per unit volume
- k : coefficient to be determined based on admixture material
- Fly ash: $k=0$, ground granulated blast furnace slag: $k=0.7$

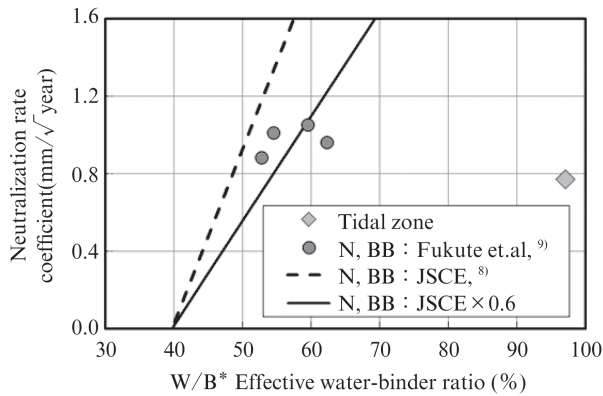


Fig. 6 Neutralization rate coefficient of a sample at tidal zone

Slaked lime: $k=1.0$, lime dust: $k=0.5$

Figure 6 shows the results when the neutralization rate coefficient is arranged with the effective water/binder ratio W/B^* on the x -axis. Fukute et al. investigated various types of concrete that were exposed for 20 years in the tidal zone, and reported that the neutralization rate is smaller than that in the atmosphere on land⁹⁾. Among these neutralization rates, the same figure shows the values for concrete using N and BB, which were made by using tap water. The JSCE neutralization rate coefficient equation⁸⁾ and the result when that equation is multiplied by 0.6 are also shown in the figure. As pointed out by Fukute et al., the neutralization rate coefficient of concrete exposed in a tidal zone is small in comparison with the JSCE equation, which is applied in the atmosphere on land, and in spite of variations, is roughly 0.6 times the result by the JSCE equation. Similarly, it can also be understood that the neutralization rate coefficient of the artificial stones exposed in the tidal zone is small in comparison with these results, indicating that neutralization was retarded. In order to further heighten resistance to neutralization, use of slaked lime or lime dust as a substitute for fly ash, etc. is considered effective.

3.5 Pore Size Distribution

The pore size measurement results are shown in **Table 3**, and the volumetric distribution by pore size is shown in **Fig. 7**. Among the pore sizes of the samples,

Table 3 Pore size measurement results of samples at tidal zone and undersea zone

Measurement item		Tidal zone		Undersea zone	
		0-10 mm	40-50 mm	0-10 mm	40-50 mm
Total pore volume	ml/g	0.156	0.178	0.128	0.136
Total pore specific surface	m ² /g	65.9	57.6	50.7	46.3
Porosity	%	27.5	32.2	25.0	26.7

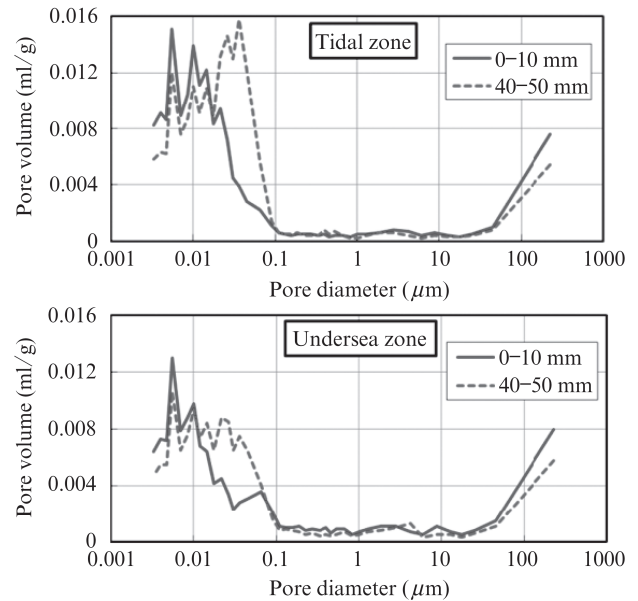


Fig. 7 Pore volume distribution of samples at tidal zone and undersea zone

the region smaller than $0.05\text{--}0.1\ \mu\text{m}$ occupied the larger part. Pores in concrete are classified mainly as capillary pores larger than $0.05\text{--}0.1\ \mu\text{m}$ (space in which precipitation of hydrates is possible), and gel pores smaller than $0.05\text{--}0.1\ \mu\text{m}$ (in which hydrates cannot precipitate)¹⁰⁾. In comparison with Portland cement, it has been reported that the amount of capillary pores decreases greatly with material age and long-term strength increases in concrete using Portland blast-furnace slag cement¹¹⁾. It can be conjectured that this is due to the effect of the high use ratio of ground granulated blast furnace slag in the iron and steel slag hydrated matrix on refinement of the pore structure and strength development after a long period of time.

With increasing depth from the sample surface, the number of pores with sizes of $0.02\text{--}0.1\ \mu\text{m}$ increases, and the total pore volume and pore ratio are large. In the depth region of $0\text{--}10\ \text{mm}$, where the effect of neutralization is considered to occur, both the total pore volume and the total pore specific area are larger in the tidal zone than in the undersea zone. It is estimated that neutralization proceeds more strongly in the tidal zone than in the undersea zone, and this results in progress of pore formation by eluviation of calcium hydroxide.

When pores in concrete are shielded by water, penetration of carbon dioxide gas is obstructed and the neutralization rate is slow. In general, evaporation of rainwater, seawater or other water that penetrates into concrete becomes more difficult as the pore size becomes smaller, and as a result, neutralization is difficult. Thus, as described above, there is no contradiction between the results of the pore size distribution and the result that steel slag hydrated matrix has excellent resis-

Table 4 Mineral phase of samples at tidal and undersea zone

Mineral phase	Tidal zone		Undersea zone	
	0-10 mm	40-50 mm	0-10 mm	40-50 mm
Calcite: CaCO_3	⊙	⊙	⊙	⊙
Vaterite: CaCO_3	△	—	△	—
Friedel's salt: $3\text{CaO} \cdot (\text{Al}_2\text{O}_3) \cdot \text{CaCl}_2 \cdot 10\text{H}_2\text{O}$	○	—	○	⊙
Hydrotalcite: $\text{Mg}_4\text{Al}_2(\text{OH})_{12}(\text{CO}_3) \cdot 4\text{H}_2\text{O}$	○	○	○	—
Calcium hydroxide: $\text{Ca}(\text{OH})_2$	—	○	—	⊙
Hydroxyapatite: $\text{Ca}_5(\text{PO}_4)_3(\text{OH})$	○	○	○	○
Ettringite: $3\text{CaO} \cdot \text{Al}_2\text{O}_3 \cdot 3\text{CaSO}_4 \cdot 32\text{H}_2\text{O}$	○	○	○	○
Magnetite: Fe_3O_4	○	△	○	○
Hematite: Fe_2O_3	○	△	○	○
Akermanite: $2\text{CaO} \cdot \text{MgO} \cdot 2\text{SiO}_2$	○	○	○	○
Silicon dioxide: SiO_2	⊙	⊙	⊙	⊙

※⊙, ○, △, —: Maximum diffraction line

⊙: Over 5 000 counts, ○: 5 000~1 000 count

△: Under 1 000 counts, —: No counts

tance to neutralization, as discussed in the previous section.

3.6 Powder X-ray Diffraction (XRD)

The results of the powder X-ray diffraction test are shown in Table 4. Ettringite, which contains S, was detected in all of the samples. Because the binder does not include gypsum, it appears that this substance was formed by the action of sulfur ions in the seawater. It also seems that SiO_2 originates from unreacted fly ash. In all of the samples, a gradual rise (halo) was observed at around $25\text{--}35^\circ$, suggesting the existence of amorphous material. The features of each exposure environment are described in the following.

- Tidal zone: The calcium hydroxide that was confirmed at “40–50 mm” was not observed at “0–10 m.” At “0–10 mm,” it is considered that calcium hydroxide was changed to calcite or vaterite by neutralization. Friedel's salt, which is a hydrate that contains Cl due to the effect of seawater, was detected at “0–10 mm.”
- Undersea zone: Friedel's salt was detected at both “0–10 mm” and “40–50 mm,” and furthermore, its intensity was stronger at “40–50 mm.” This is thought to be because Cl diffusion advanced to a depth of “40–50 mm,” resulting in the formation of Friedel's salt, which is a hydrate that contains Cl, to this depth, while Friedel's salt decreased due to eluviation from the “0–10 mm” depth region on the surface side.

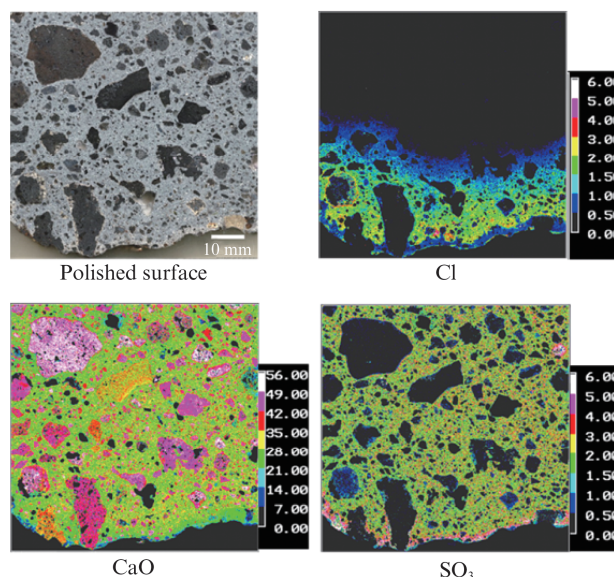


Fig. 8 Elemental distribution of a sample at tidal zone

3.7 Elemental Distribution

The results of an EPMA area analysis of a tidal zone sample are shown in Fig. 8. Except for Cl, all elements have been converted to the oxide state (shown as%). Cl has penetrated substantially in parallel with the surface to a depth of about 30–40 mm. Both CaO and Cl are low in the region 1–3 mm from the sample surface, which seems to be the result of formation and eluviation of Friedel's salt. Although SO_3 is roughly uniform in most of the matrix, this is thought to be due to the conversion of the S in the ground granulated blast furnace slag to SO_3 . In addition, SO_3 is low in the dark brown region at the extreme surface and high in the region that appears white to the eye in the region inside the outer surface. A SO_3 concentration phenomenon in which Ettringite is decomposed by neutralization, the sulfate ions released in this process shift to the uncarbonated region due to the concentration gradient, and regions of high SO_3 concentration form locally is frequently recognized in concrete¹²⁾. In the X-ray diffraction results, a larger amount of calcium carbonate, which appears to have formed by neutralization, was observed in the “0–10 mm” region than in the “40–50 mm” region. Accordingly, it can be thought that the SO_3 concentration phenomenon has proceeded in the iron and steel slag hydrated matrix in the same manner as in concrete.

4. Conclusion

The properties of iron and steel slag hydrated matrix were investigated after exposure in a sea area for approximately 10 years. The following results were obtained.

- (1) A large number of marine organisms such as lug-worms, starfish, barnacles, etc. were found on the surface of the samples exposed in the sea immediately after the samples were recovered.
- (2) Compressive strength increased with time. After 10 years, compressive strength was 27–30 N/mm², which was more than two times higher than at the time of manufacture.
- (3) Chloride penetration was more pronounced in the undersea zone than in the tidal zone. The apparent Cl diffusion coefficient was 0.04–0.16 cm²/yr in the tidal zone, which is similar to or less than that of concrete using Portland blast-furnace slag cement. In the undersea zone, the Cl diffusion coefficient was 0.3–0.5 cm²/yr, which was an intermediate level between that of concrete using ordinary Portland cement and concrete using Portland blast-furnace slag cement.
- (4) The average neutralization depth in the tidal zone was 2.5 mm, and the neutralization rate coefficient was small in comparison with that of ordinary concrete.
- (5) The pore size was small, which was consistent with the result that iron and steel slag hydrated matrix has excellent neutralization resistance. It can be conjectured that the high use ratio of ground granulated blast furnace slag influenced both refinement of the pore structure and strength development.
- (6) As in the case of concrete, formation and eluviation of Friedel's salt and concentration of SO₃ were confirmed in iron and steel slag hydrated matrix.
- (7) As artificial stones made from iron and steel slag hydrated matrix have a good adhesion property for marine organisms as well as stable mechanical properties, the possibility of stable application as a stone material for marine applications was confirmed. The results of an investigation of chloride penetration, neutralization, pore size distribution, formed mineral phases and the elemental distribution confirmed that this material has properties equal or superior to those of marine concrete using ordinary Portland cement or Portland blast-furnace slag cement.

References

- 1) Matsunaga, H.; Kogiku, H.; Takagi, M.; Tanishiki, K. *Concrete Journal*. 2003, vol. 41, no. 4, p. 47–54.
- 2) Matsunaga, H.; Tanishiki, K.; Tsujimoto, K. *JFE Technical Report*. 2009, no. 13, p. 53–57.
- 3) Udagawa, E.; Matsunaga, H. *JFE Gihō*. 2008, no. 19, p. 18–22.
- 4) Sakoda, S.; Yamane, C.; Takeda, Y. *Proceedings of the Japan Concrete Institute*. 2003, vol. 25, no. 1, p. 707–712.
- 5) Yamaji, T.; Tarek Uddin Mohammed, Aoyama, T.; Hamada, H. *Proceedings of the Japan Concrete Institute*. 2001, vol. 23, no. 2, p. 577–582.
- 6) Japan society of civil engineers. *Standard Specifications for Concrete Structures -2012 -Design-*. 2012, p. 148–155.
- 7) Yamaji, T. *Technical note of the port and airport research institute*. 2011, no. 1232, p. 85–95.
- 8) Japan society of civil engineers. *Standard Specifications for Concrete Structures -2012 -Design-*. 2012, p. 147–148.
- 9) Fukute, T.; Hamada, H.; Yamamoto, K. *Journal of Japan Society of Civil Engineers*. 1992, vol. 16, no. 442, p. 43–52.
- 10) Nakai, K.; Ishida, T.; Kishi, T.; Maekawa, K. *Journal of Japan Society of Civil Engineers*. 2005, vol. 69, no. 802, p. 61–78.
- 11) Sagawa, T.; Ishida, T.; Yao Luan.; Nawa, T. *Journal of Japan Society of Civil Engineers*. 2010, vol. 66, no. 3, p. 311–324.
- 12) Kobayashi, K.; Shiraki, R.; Kawai, K. *Concrete Research and Technology*. 1990, vol. 1, no. 2, p. 69–82.